

Contribution to the Full 3D Finite Element Modelling of a Hybrid Stepping Motor with and without Current in the Coils

Belemdara Dingamadji Hilaire¹, Mbainäibeye Jérôme², Guidkaya Golam³

¹Department of Physics and Engineering Sciences, University of N'Djamena, N'Djamena, Chad

²Department of Physics, University of Moundou, Moundou, Chad

³Department of Physics, University of Ngaoundere, Ngaoundere, Cameroon

Email: hbelemdara@gmail.com

How to cite this paper: Hilaire, B.D., Jérôme, M. and Golam, G. (2024) Contribution to the Full 3D Finite Element Modelling of a Hybrid Stepping Motor with and without Current in the Coils. *Journal of Electromagnetic Analysis and Applications*, 16, 11-23.

<https://doi.org/10.4236/jemaa.2024.162002>

Received: January 14, 2024

Accepted: February 26, 2024

Published: February 29, 2024

Copyright © 2024 by author(s) and Scientific Research Publishing Inc. This work is licensed under the Creative Commons Attribution International License (CC BY 4.0).

<http://creativecommons.org/licenses/by/4.0/>



Open Access

Abstract

The paper presents our contribution to the full 3D finite element modelling of a hybrid stepping motor using COMSOL Multiphysics software. This type of four-phase motor has a permanent magnet interposed between the two identical and coaxial half stators. The calculation of the field with or without current in the windings (respectively with or without permanent magnet) is done using a mixed formulation with strong coupling. In addition, the local high saturation of the ferromagnetic material and the radial and axial components of the magnetic flux are taken into account. The results obtained make it possible to clearly observe, as a function of the intensity of the bus current or the remanent induction, the saturation zones, the lines, the orientations and the magnetic flux densities. 3D finite element modelling provide more accurate numerical data on the magnetic field through multiphysics analysis. This analysis considers the actual operating conditions and leads to the design of an optimized machine structure, with or without current in the windings and/or permanent magnet.

Keywords

Modelling, 3D Finite Elements, Magnetic Flux, Hybrid Stepping Motor

1. Introduction

Electronics and computer science have grown considerably in recent decades. They make possible the design, multiphysics analysis of electromagnetic phenomena and parameter optimization in electrical machines. The analytical method

and the 2D finite element method have led to better results in radially excited electrical machines only. Hybrid variable stepping motors, in addition to the interaction of the radial field and the axial field, have a variable air gap geometry [1]. The axial field and the variable geometry make it difficult to study analytically and even numerically in 2D as soon as the local iron saturation is not negligible [1]-[6]. However, the 3D finite element method, which was once considered time and space consuming, is possible and reported in this paper. This finite element approach is possible thanks to the COMSOL Multiphysics software interacting with Matlab which allows to save time and to obtain a better accuracy by taking into account the 3D nature, the local iron saturation as well as the air gap geometry.

In this paper, we analyze the electromagnetic phenomena by the 3D finite element method applied to the hybrid stepping motor. The variables manipulated are the bus current and the remanent magnetic induction. The objective of this study is to establish the magnetic maps and the flux graphs of the phases, which maps will allow to highlight the radial and axial field depending on whether there is the presence of the permanent magnet or not, whether there is the presence of the current or not, depending on whether both quantities act simultaneously. The rest of this paper is organized as follows: Section 2 presents the materials and methods; the results of the 3D modelling with and without current, with and without remanent induction are presented in Section 3. Section 4 presents the results in terms of the magnetic flux pattern of the phases. Discussions on the results of this work are presented in section 5 and 6. Finally, the conclusion and perspectives are presented in section 7.

2. Materials and Methods

2.1. Materials

2.1.1. Structure of Hybrid Stepping Motor

The hybrid stepping motor studied **Figure 1** is doubly salient with 50 teeth on the rotor and 5 teeth on each of the 8-stator pads forming the four phases. It consists of two coaxial half-machines with two rotor rings **Figure 2** mechanically offset by half an electrical period and two half-stators juxtaposed through a permanent magnet. The two coaxial half stators are electrically linked since their two superimposed pads carry the same winding and mechanically linked since the interposed magnet closes the magnetic flux circuit [1] [4] [7] [8]. The ferromagnetic material used is a lossless iron and there are no hysteresis effects. The permanent magnet used has a remanent density B_r of 1.42 T. **Table 1** gives less dimensions studied motor.

2.1.2. Material Constitutive Relationship

The material used is iron without magnetic loss, characterized by its first magnetization curve as shown in **Figure 3**. The local saturation of this material is taken into account through the constitutive relations mentioned by Equation (1). This characteristic has three zones: the linear zone (OA) which corresponds to the

remanent induction, the saturation bend (AB) where the ferromagnetic material is supposed to be exploited to its full potential [4] and the saturation zone (BC) where the magnetic induction is almost constant. This characteristic provides information about the magnetic properties of iron and how it can be used to build electrical machines. Taking into account this characteristic of iron allows manufacturers to optimise the design of electrical machines to improve efficiency and reduce energy losses.

Table 1. Dimensions of the hybrid stepping motor studied.

Designation value	Value
Outside radius	26.9 [mm]
Stator bore radius	14.845 [mm]
Rotor radius	14.77 [mm]
Non-magnetic shaft radius	11.2 [mm]
Stator yoke height	2.5 [mm]
Height of stator yoke	7 [mm]
Height of stator pole spread	1.25 [mm]
Magnet inner radius	24.4 [mm]
Air gap thickness	0.075 [mm]
Magnet height	2.540 [mm]
Stator pad width	5 [mm]
Effective length per half machine	7.5 [mm]
Radius of the tooth gap	0.25 [mm]
Rotor duty cycle	0.335
Stator duty cycle	0.345
Number of stator pads	8
Number of rotor teeth	50

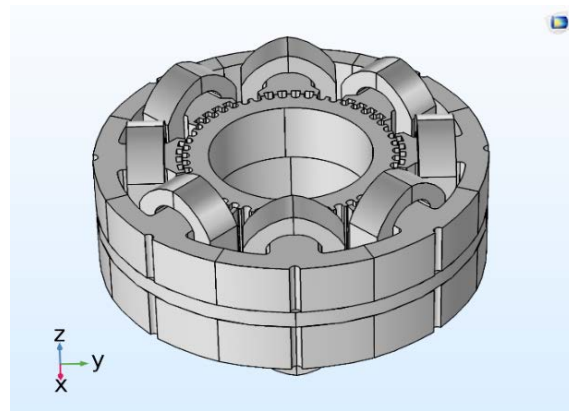


Figure 1. Geometry of a hybrid stepping motor.

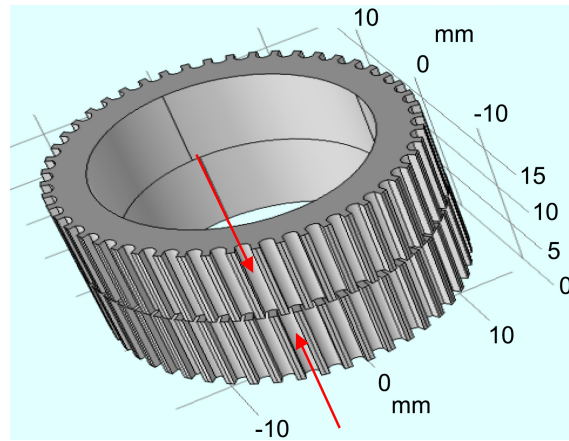


Figure 2. Twisted rotor.

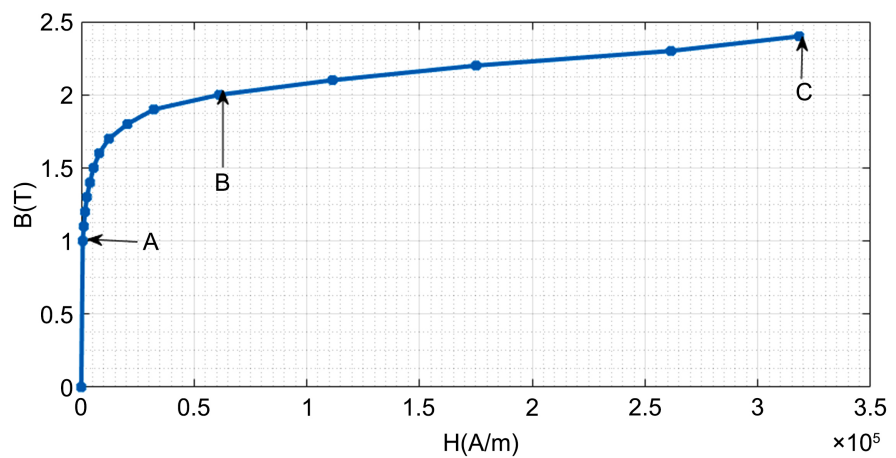


Figure 3. First magnetization curve.

This non-linearity of the material is taken into account by the choice of the constitutive relation related to the following HB curve:

$$H = f(|B|) \frac{B}{|B|} \tag{1}$$

2.1.3. Characteristics of the Permanent Magnet

The addition of the permanent magnet between the two half stators compensates for the excessively high input but distances the machine from the pure structure. The machine has a holding torque on its axis and therefore a position memory. The value of this torque depends on the remanent induction and the volume of the permanent magnet. However, a large volume of magnet can affect the useful length of the machine and therefore reduce its power density [9] [10]. Neodymium iron boron (Figure 4) is characterised by the remanence or magnetic strength that remains after demagnetization and the intrinsic coercive field or current required for demagnetizing the magnet. The field strength required to demagnetize neodymium iron boron is approximately 2800 kA/m. This field strength is smaller for other types of magnets, some 1200 to 1400 kA/m.

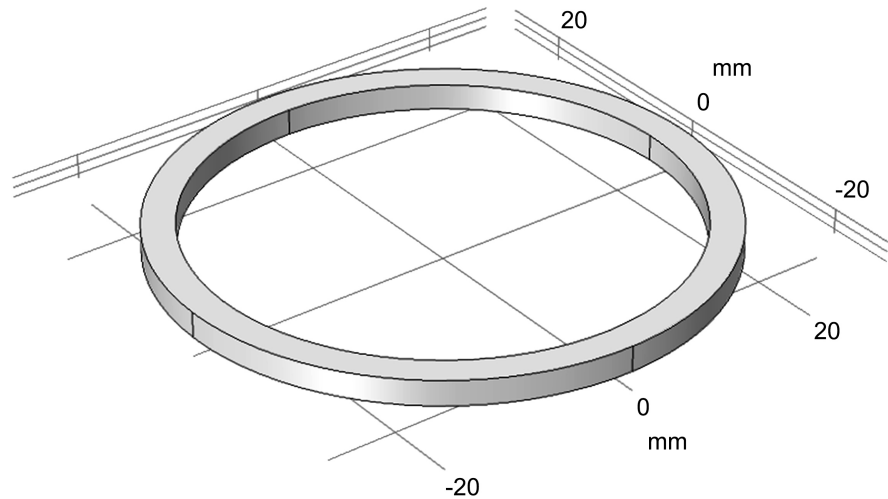


Figure 4. Permanent magnet.

One of the qualities of this permanent magnet is its operating temperature (80° and 300°) which has an upper limit and the curing temperature at which it loses its properties (310° and 330°) [11].

2.2. Methods

2.2.1. Identification of the Finite Element Model Parameters

The following steps precede the finite element analysis for the machine modeling:

- The construction of the machine geometry in 3D by programming with the COMSOL software associated with the Matlab calculation environment using the “bezier” geometry;
- The choice of materials such as copper for the coils, the permanent magnet and iron without magnetic losses, taking into account the non-linearity;
- The realization of an adequate mesh;
- The choice of the magnetic field as the study physics;
- The calculation of finite elements.

The calculation of the field (magnetic vector potential) is done by coupling and exploiting the evolution and conservation laws given by Equations (1), (2) and (3), which allow the establishment of the electromagnetic field model governed by Equations (2), (3), (4) and (5):

$$\nabla H = J \quad (2)$$

$$B = \mu_0 \mu_r H = \nabla A \quad (3)$$

$$J = \sigma E \quad (4)$$

$$\nabla \left(\frac{1}{\mu} \nabla A \right) = J + \nabla \left(\frac{1}{\mu} \nabla B_r \right) \quad (5)$$

where:

H : is the magnetic field strength;

B : is the magnetic flux density;

- B_r : is the remanent induction;
- A : is the magnetic vector potential;
- μ_0 : is the vacuum permeability;
- μ_r : is the relative permeability of the material
- J : is the current density;
- E : is the electric field;
- σ : is the electrical conductivity.

In order to determine the magnetic field distribution in the machine, an assumption is made that the magnetic field is zero outside the bounding box and that the magnetic vector potential is zero ($A = 0$) at the peripheral surface of the motor [5].

2.2.2. Coil Geometry Analysis

The material used for the machine windings is copper. The conductor design is a homogenised multi-coil type. The windings are carried by each of the 8 stator pads offset from each other by $\pi/4$. In order to maximise the average torque, the windings are interconnected in additive flux. This interconnection is achieved between the coils (Figure 5) carried by the diametrically opposed pads in pairs forming a phase. The characteristics of the copper material are presented in Table 2.

The windings of the machine are by Equation (5) which expresses the current density (J) as a function of the number of turns per unit length, the current flowing in the windings (I_{coil}) and the magnetic vector potential (A). It is important to characterise the coil by the current density which can affect the conductivity of the coil, as well as its capacitance and inductance. Indeed, the higher the current density, the higher the electrical resistance of the coil, which can lead to overheating and deterioration. Current density should be taken into account when designing and using coils.

$$J = \frac{NI_{coil}}{A} \tag{6}$$

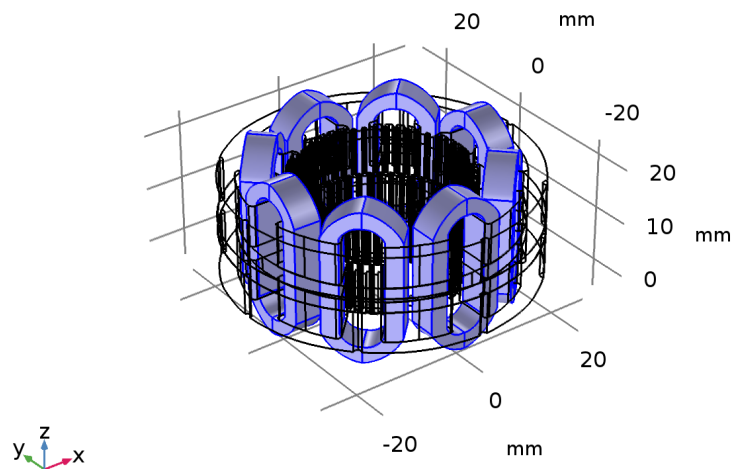


Figure 5. Coil geometry.

Table 2. Coil parameters.

Name	Value	Unit
Relative permeability	1	
Relative permeability	1	
Electrical conductivity	8.998×10^7	S/m
Thermal conductivity	400	W/m·K
Heat capacity at constant pressure	385	J/kg·K
Surface emissivity	0.5	
Reference temperature	293.15	K
Reference resistivity	1.667×10^{-8}	$\Omega \cdot m$
Temperature dependent coefficient of resistivity	3.862×10^{-3}	K^{-1}

2.2.3. Meshing

Figure 6 shows the mesh of the 3D geometry of the hybrid variable reluctance machine in (x, y, z) space.

Table 3 shows the finite element characteristics of the hybrid stepping motor mesh in terms of fineness and type of elements. The size is expressed in millimeters (mm). The mesh size is adapted according to the areas of interest. Thus, the smallest elements are found in the air gap, but the coarse mesh is applied everywhere else. The finer the mesh size, the more accurate the results.

3. Magnetic Flux Results

Figure 7, **Figure 9** and **Figure 10** show the results obtained in terms of magnetic flux density without current and with remanent induction, with current and without remanent induction, and with current and remanent induction respectively.

3.1. Magnetic Flux Density without Current and with Residual Induction

Figure 7 displays a stepping machine magnetic card without electricity supply. The magnetic field source is a permanent magnet **Figure 8** with a remanent induction. The figure illustrates the field's circulation direction and magnetic flux density.

3.2. Magnetic Flux Density with Current and without Remanent Induction

Figure 9 shows a stepping machine magnetic card when an electric current is applied. However, it does not have a permanent magnet. The magnetic characteristics shown in this figure are those of a double saliency variable reluctance machine in terms of magnetic field circulation and density.

Table 3. Mesh statistics.

Description	Value
Minimum element quality	0.003305
Average quality of elements	0.6057
Tetrahedron elements	286,837
Triangular elements	62,926
Edge elements	15,707
Point elements	2500

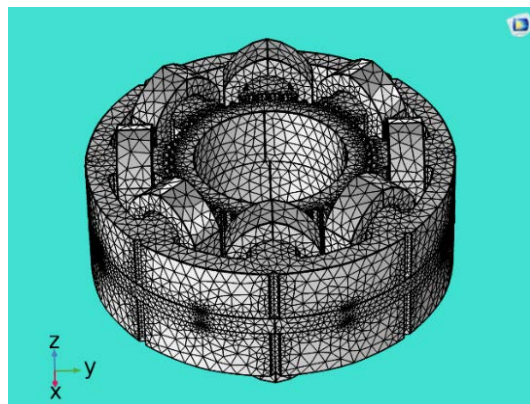


Figure 6. Geometry mesh.

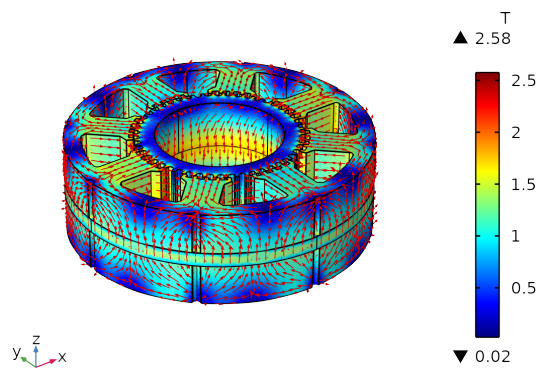


Figure 7. Magnetic flux density for $I = 0A$ and $Br = 1.42T$.

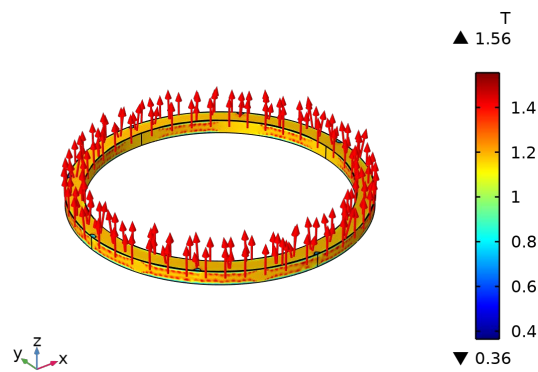


Figure 8. Axial field source.

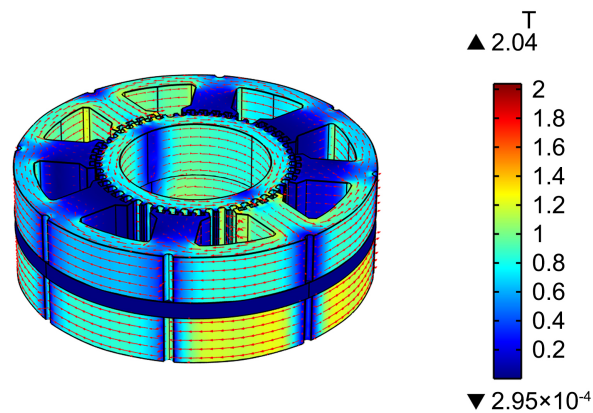


Figure 9. Magnetic flux density for $I = 1\text{ A}$ and $B_r = 0\text{ T}$.

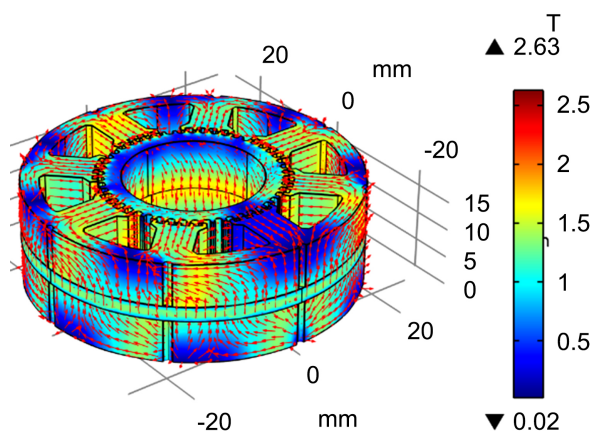


Figure 10. Magnetic flux density for $I = 1\text{ A}$ and $B_r = 1.42\text{ T}$.

3.3. Magnetic Flux Density with Current and Remanent Induction

Figure 10 displays a hybrid variable reluctance machine magnetic card. It has two field sources: the electric current in the windings and the permanent magnet. It has two field sources: the electric current in the windings and the permanent magnet. The figure illustrates the combined effect of these two sources of field strength.

4. Phase Flux Results

Figure 11 shows the plots of the additive and concatenated coil fluxes per phase without considering the permanent magnet, as a function of rotor position. Figure 12 shows the concatenated coil fluxes per phase added to the magnet flux, as a function of rotor position.

5. Discussions on the Magnetic Flux Density

Figure 7 is a magnetic map of the hybrid stepping motor where only the permanent magnet with a residual density of 1.42 T is the only source of flux. In this

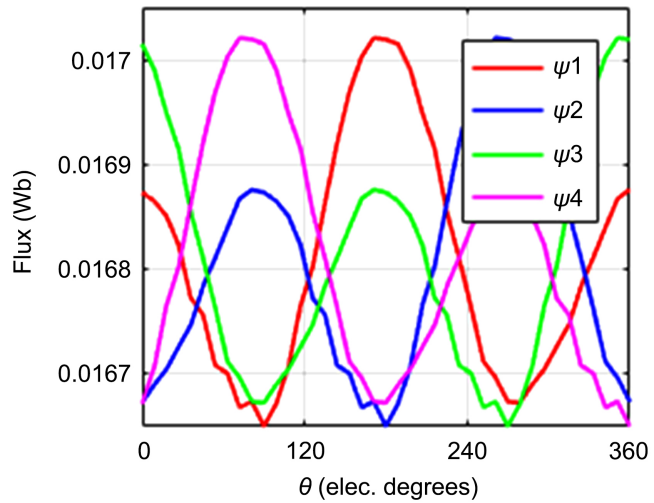


Figure 11. Phase flux without magnet.

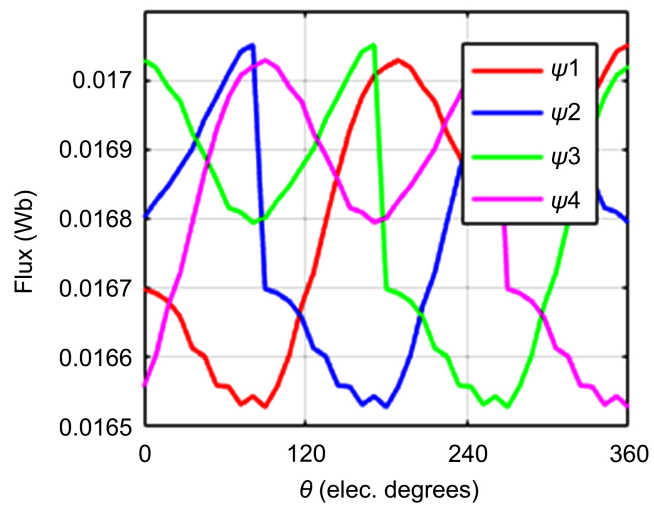


Figure 12. Phase flux with magnet.

figure, the local saturation of the iron can be clearly seen. It is therefore a function of the position of the rotor. Thus, at the level of the rotor teeth opposite the stator teeth (conjunction position), the magnetic saturation is denser, about 2.58T. This saturation is less dense when the teeth of the two armatures are in opposition position, about 0.02T. We also observe a low saturation in the middle of the stator yoke separating two stator pads. This low local density is due to the deflection of the flux channeled to reach the rotor through the pads. The areas close to the magnet are also saturated but at intermediate values between the extreme values marked on the graphic legend of this figure. The field lines run along the axis of the machine. Channeled by the iron, these lines leave the permanent magnet, enter the first half-stator, and return through the rotor and the second half-stator. These field lines hardly reach the unsaturated zones. This path of the magnetic field shows that the magnet closes its field lines. The circulation of the magnetic flux through the two half-machines shows the symmetry

of its polarity [1] [6].

Figure 9 is a magnetic map of a hybrid stepping motor where the injection of the 1A bus current into the coils generates the magnetic flux. This figure shows the magnetic saturation along the stator yokes and on the fed phase pads. This magnetic saturation becomes more pronounced at the diametrically opposed stator pads that form the current-supplied phase at that moment. Even if two stator pads carry the same winding, their magnetic saturation levels differ. This difference is due to the twisting of the rotor making one of the pads with teeth superimposed in opposition and the other pad with teeth in conjunction. The graphical legend shows that the density of the magnetic induction can reach a maximum value of 2.04T at the level of the teeth in conjunction corresponding to the phase supplied at that moment. This density is only 2.95×10^{-4} T precisely at the level of the pads of the other three non-powered phases.

The lines describe a radial field flow and their paths show that the concatenated fluxes of the coils are additive. For a half-stator, the field flows along the stator yoke into one pad of the supplied phase and out the diametrically opposite pad.

Figure 10 is a magnetic map of a hybrid stepping motor obtained when both sources of flux (electric current and permanent magnet) exist. The injected bus current is 1A for a residual induction (Br) of 1.42T. The saturations on the ferromagnetic material result from the simultaneous actions of the permanent magnet and the current in the coils. The most saturated areas are the pads of the energized phases and those with teeth in conjunction with those of the rotor. The maximum value of the magnetic induction in these areas is 2.63T while the minimum is 0.02T. This maximum value of magnetic induction is much higher than those obtained by the injection of electric current or by the addition of the permanent magnet separately mentioned above. This figure shows the contribution of the two flux sources (current and permanent magnet) in terms of magnetic flux density in view of the graphical legend. In addition, no study that does not consider both sources of flux can claim to give a better local approximation of the flux.

This map (**Figure 10**) shows lines corresponding to the axial and radial components of the magnetic flux. The axial flow of the flux is of purely reluctant origin [7] [8] [12] whereas the radial magnetic flux is induced by the coils of the phase supplied with electric current. The coexistence of these two sources in this machine makes it impossible to study them analytically and even numerically in 2D since they cannot take into account the axial components of the magnetic flux. Indeed, the hybrid term originates from these two sources of magnetic field.

6. Discussions on the Magnetic Flux Curve of the Phases

The power supply sequence for this hybrid variable reluctance machine is 4-3-2-1. Each coil has 200 turns.

Like all stepper machines, the phases of a hybrid variable reluctance machine are independent of each other [9] [10]. Therefore, they are fed in succession and there is no mutual flux between phases.

In **Figure 11**, when phase 4 is energized, the teeth of the pins of the first half-machine are in the joint position. This phase sees its flux (ψ_4) reach its maximum amplitude, which is 0.017 Wb. It is followed by phase 2 in terms of flux amplitude. In fact, phase 2, although not supplied with current at that moment, has a higher flux amplitude than the last two (ψ_1 and ψ_3) because of the rotor twist. The rotor twist causes the teeth of the stator pads of the second half to align with those of the rotor. This state of phase 2 shows that the flux follows the air gap permeances. As for the fluxes of phases 1 and 3 (ψ_1 and ψ_3), they are in the low state, which shows that the teeth of the stator pads carrying these phases, which are not powered at this moment, are in the opposition position. This situation described is reversed in the second half of the electrical period, *i.e.* from 180° to 360° . We also notice that it is the opposition positions that are the seats of the phase flux ripples. The low phase flux ripples are observed for flux values below 0.0168 Wb.

In **Figure 12**, two sources of flux, namely the current and the magnet, are present; thus, for a current-fed phase, the flux value oscillates between a maximum of over 0.017 Wb and a minimum of 0.0168 Wb. However, as soon as the phase current is switched off, the flux drops vertically to 0.0166 Wb and then evolves to end the period.

We can say that all the curves observed below 0.0166 Wb are those of magnet flux. On these portions of the curves, there are strong undulations.

The sharp rises and falls in the curves are caused by the sequence of commands to apply and remove current in a phase. The sawtooth curves in **Figure 10** represent the magnetic field passing through the two armatures as a function of rotor position. The hybrid machine applies current to generate the magnetic field.

7. Conclusion and Perspectives

The full 3D Finite Element Method applied to the hybrid stepping motor has allowed the calculation of the field with current in the coils. The magnetic maps obtained show the local iron saturations as well as the radial and axial flux flow. The contribution of the magnet and coil fluxes to the concatenated magnetic flux of the two sources shows that neither source can be neglected in the study of this hybrid machine. The flux curves show that by injecting only the current, there is less ripple. For the supplied phase, the minimum flux value can be less than 0.0167Wb. However, when there is the current and the permanent magnet, the minimum flux value is greater than or equal to 0.0168 Wb. By switching off the current in this phase, the minimum flux value falls below 0.0167 Wb where strong ripples exist. The ripples of the electromagnetic quantities are of quasi-reluctant origin.

In the future, we plan to evaluate this 3D model of the hybrid stepping motor in order to study its static and dynamic behavior.

Conflicts of Interest

The authors declare no conflicts of interest regarding the publication of this paper.

References

- [1] Fankem, E.D.K., Takorabet, N., Meibody-Tabar, F. and Sargos, F.M. (2010) Nonlinear Finite Element-Circuit Model of a Hybrid Stepping Motor. *COMPEL: The International Journal for Computation and Mathematics in Electrical and Electronic Engineering*, **29**, 957-963. <https://doi.org/10.1108/03321641011044370>
- [2] Lim, K.C., Hong, P. and Kim, H.-T. (2001) Characteristics Analysis of 5 Phase Hybrid Stepping Motor Considering the Saturation Effect. *IEEE Transactions on Magnetics*, **37**, 3518-3521. <https://doi.org/10.1109/20.952651>
- [3] Lu, B.L., Xu, Y.L. and Ma, X. (2016) Design and Analysis of a Novel Stator Permanent-Magnet Hybrid Stepping Motor. *IEEE Transactions on Applied Superconductivity*, **26**, Article No. 0607705. <https://doi.org/10.1109/TASC.2016.2594868>
- [4] Ramu, K. (2001) Switched Reluctance Motor Drives: Modeling, Simulation, Design and Applications. CRC Press, Boca Raton.
- [5] Lindsay, J.F., Arumugam, R. and Ramu, K. (1986) Finite-Element Analysis Characterisation of a Switched Reluctance Motor with Multitooth Per Stator Pole. *IEE Proceedings*, **133**, 347-353. <https://doi.org/10.1049/ip-b.1986.0046>
- [6] Hilaire, B.D. (2019) Méthodes des éléments finis 3D et le couple de denture d'une machine à réluctance variable hybride. Editions universitaires européennes, Amazon.
- [7] Peng, Z., Bi, C., Fang, L. and Xiao, L. (2022) Optimization of the Three-Phase Stepper Motors for Noise Reduction. *Sensors*, **22**, Article 356. <https://doi.org/10.3390/s22010356>
- [8] Fan, Y.Y. (2019) 3D Finite Analysis of a Hybrid Stepper Motor. Degree Project in Electrical Engineering, Stockholm.
- [9] Girardin, M. (2000) Modélisation et réglage d'un entraînement à haute performance par un moteur réluctant. Ph.D. Thesis, Ecole Polytechnique Fédérale de Lausanne, Lausanne.
- [10] Multon, B. (1994) Conception et alimentation électronique des machines à réluctance variable à double saillance. HDR, Omaha.
- [11] Buss, S. (2010) Aimants Permanents et Assemblages intégrés. YX Magnetic SA. <http://www.yxmagnetic.com>.
- [12] Kenmoe, E.D. (2012) Etude de différentes structures d'actionneurs de positionnement pour l'aéronautique. Ph.D. Thesis, Université de Lorraine, Lorraine.